RSC Medicinal Chemistry

ROYAL SOCIETY OF CHEMISTRY

RESEARCH ARTICLE

Published on 11 September 2026
Licence and permissions

Check for updates

Cite this: DOI: 10.1039/d6md00313c

Site-selective acylation of human insulin to engineer a long-acting monovalent insulin–Fc conjugate

Wanrong Yang, Ruolin Xu and Wanyi Tai *

Received 21st April 2026,
Accepted 10th September 2026

DOI: 10.1039/d6md00313c

rsc.li/medchem

Basal insulin therapy requires sustained and low-variability of insulin exposure; however, natural human insulin is rapidly cleared, thus necessitating frequent subcutaneous injections. Here we report a modular chemical platform for constructing monovalent insulin–Fc conjugates with structural homogeneity and long-term action. Site-selective acylation on three accessible amines of insulin (Gly^{A1}, Phe^{B1}, or Lys^{B29}) yields a panel of alkynyl insulin analogs (**3a**–**3c**), which could couple with an azido Fc protein by CuAAC to produce monovalent insulin–Fc conjugates. Among these conjugates, Fc conjugation at Lys^{B29} of insulin, namely **3c**–Fc, retains the bioactivity, while insulin at Gly^{A1} (**3a**–Fc) and Phe^{B1} (**3b**–Fc) were markedly deactivated, as assessed by the downstream Akt phosphorylation test. *In vivo*, the **3c**–Fc conjugate exhibits a long pharmacokinetic and pharmacodynamic profile, which may result from the increase in the molecular size, the recycling by the neonatal Fc receptor, and the monovalence for slow insulin receptor-mediated clearance. Overall, we describe here the method of site-selective acylation and Fc conjugation to tune the basal-leaning pharmacology of insulin.

Introduction

Diabetes mellitus (DM) is a major non-communicable disease, with the global prevalence increasing from 135 million individuals in 1995 to nearly 600 million by 2025.[1] For patients with type 1 DM and some with advanced type 2 DM, exogenous insulin is indispensable for managing normal glycemia.[2] There are currently several basal insulin products on the market for subcutaneous injections daily. The first once-weekly basal insulin, insulin icodec, was also approved by the FDA for adults with type 2 diabetes in 2026.[3,4] Patients with diabetes who require insulin would favor these long-acting insulin products, which offer convenience, adherence, and quality of life with good glucose control and long-term outcomes.[5] Therefore, efforts are still needed to further reduce the treatment burden.[6,7]

Several strategies have been proposed to elongate the duration of insulin action. These include increasing the apparent molecular size of insulin to limit renal filtration,[8] leveraging long-circulation carriers such as Fc or albumin that benefit from neonatal Fc receptor (FcRn)-mediated recycling,[9–11] and engineering the insulin moiety with reduced potency and receptor-mediated clearance.[12–14] It is noted that the lowering of *in vitro* potency does not translate into a reduction of *in vivo* potency, but instead extends the pharmacodynamic action profile of insulin.[15] Following this guideline, several groups have reported numerous attempts to develop long-acting insulin, including insulin acylation with a fatty diacid, PEGylation, microsphere formulation, and others.[4,8,16,17]

Among the concepts of designing long-acting insulins analogs, Fc conjugation or fusion is a popular strategy to reduce the renal filtration and any non-specific clearance from blood. Several groups have developed the single-chain and heterodimeric two-chain insulin–Fc fusion protein for the prolonged blood glucose control.[18,19] However, insulin potency is sensitive to the sequence and length of the connecting peptide in fusion.[20] The suboptimal designs could impede the insulin receptor engagement and even reduce the fusion protein stability.[21] Moreover, the dimeric structure of Fc protein favors a divalent insulin fusion. However, dimeric insulins of fusion protein would yield high avidity for insulin receptors, which may translate to increased receptor-mediated clearance.[22] This is considered the major clearance pathway of insulin, and can shorten the duration of insulin analogs.[23] In this regard, the chemical conjugation of insulin with Fc protein becomes a better option, with advantages such as the easy control of mono-valency, selection of conjugation site on insulin beyond the N-/C-termini, and compatibility with insulin modification, for example, the non-natural amino acid incorporation.[24]

In this context, Tagmose *et al.* from Novo Nordisk describe a chemical approach to conjugating insulin with Fc protein

Department of Pharmaceutical Engineering, School of Pharmaceutical Sciences, Wuhan University, Wuhan, Hubei 430071, China. E-mail: wanyi-tai@whu.edu.cn

using a trifunctional linker.[25] It firstly reacts with a lysine residue of insulin and then conjugates with one molecule of Fc by re-bridging the native disulfide bond *via* its two thiol reactive groups. This monovalent insulin–Fc demonstrates an ultra-long pharmacokinetic profile but shows no blood glucose-lowering activity in SD rats unless a long spacer is inserted between insulin and Fc protein. The result indicates that insulin conjugation at the disulfide bond of Fc would generate steric hindrance, limiting its accessibility to insulin receptors. In the present work, we sought to develop a complementary monovalent insulin–Fc architecture in which insulin is conjugated to the N-terminus of one Fc chain. This design was intended to control insulin valency, avoid bivalent receptor engagement, and place the insulin moiety away from the Fc dimer interface. To obtain a monovalent conjugate, we introduced a single-chain Fc precursor, which allows selective functionalization of one Fc chain with an azide group at the N-terminus. Using this scaffold, we prepared site-defined alkynyl insulin analogs at Gly^{A1}, Phe^{B1}, or Lys^{B29} and coupled them with azido Fc by CuAAC. The controlled set of conjugates allows us to examine how the conjugation site affects insulin signaling, as assessed by Akt phosphorylation, and *in vivo* pharmacodynamics. Among the three tested conjugation sites, conjugation at Lys^{B29} (**3c**–Fc) best preserves the signaling of the insulin pathway. *In vivo*, we demonstrated that **3c**–Fc shows a more sustained glucose-lowering profile than native insulin and displays a basal-like pharmacodynamic profile comparable to insulin degludec in diabetic mice.

Results and discussion

Site-selective acylation of human insulin

Human insulin consists of two interconnected peptide chains, which are commonly annotated as chain A and B, respectively (Fig. 1A). Depicting from the chemical structure, insulin possesses three primary amino groups (Gly^{A1}, Phe^{B1} and Lys^{B29}), which all are accessible by acylation and other modifications (Fig. 1B).[26] Past experience with insulin illustrated the challenge involved in the complex acylation of insulin chains.[27–31] By leveraging the differences of these amino groups in reactivity and position, we report a method of site-selective acylation of human insulin at each amino position, and the synthetic route is shown in Fig. 1C. Briefly, we employ two acylation conditions: basic aqueous conditions (pH 11.5) and organic base/DMSO conditions, to label the ε-amine (Lys^{B29}) and α-amine (Gly^{A1}, Phe^{B1}) with alkyne-PEG_3-NHS, respectively. The latter conditions involve the water-exclusive organic reaction, which is more reactive but less selective. Here we utilized the *N*-(*tert*-butoxycarbonyloxy) succinimide (Boc-NHS) protecting group to mask the feasible sites, leaving the less reactive amino group for acylation under these conditions. The profiling of acylation sensitivity reveals that the amino groups in insulin could rank in the following order: Lys^{B29} > Gly^{A1} > Phe^{B1}. Both Gly^{A1} and Phe^{B1} are α-amines, but Gly^{A1} is more solvent exposed and reactive. By tuning the base equivalence, we can achieve selective acylation at the two positions with the assistance of the Boc protecting group. The position selectivity in the acylation reaction was examined and confirmed by analytical RP-HPLC,

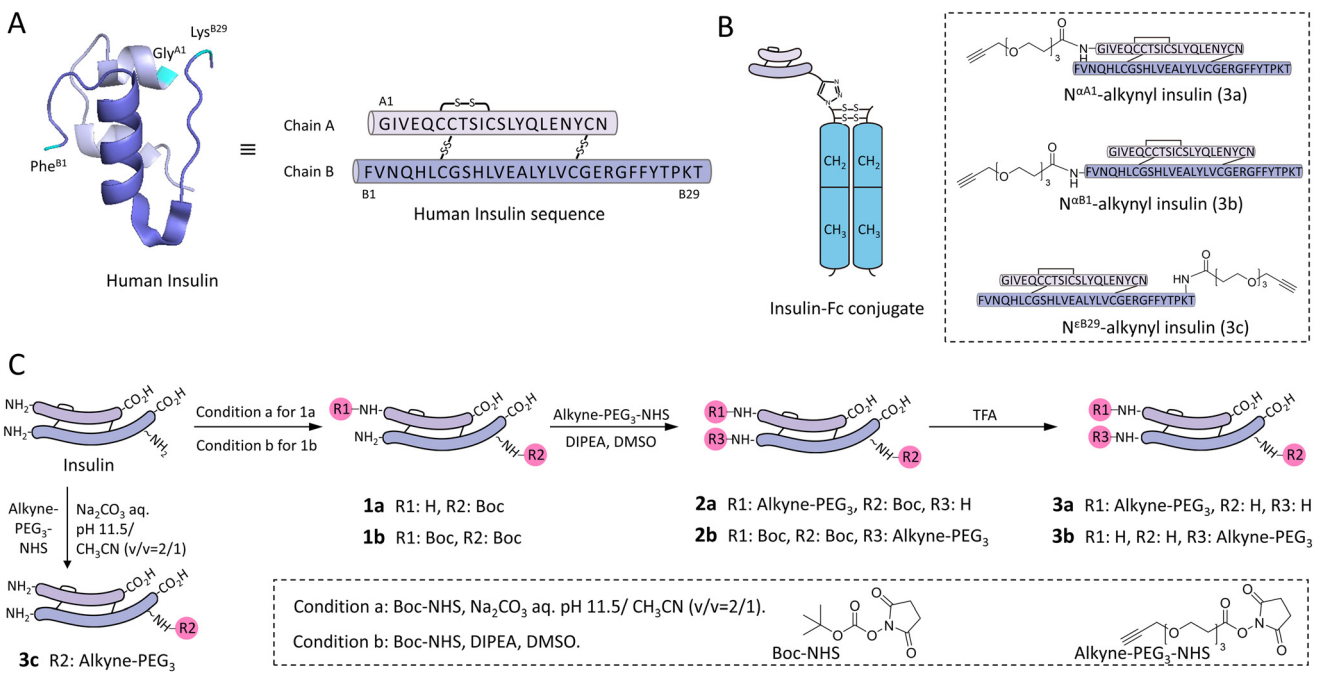

Fig. 1 Site-selective acylation of human insulin and its monovalent conjugation with Fc. (A) Illustration of human insulin structure showing the chain A and B linked by disulfide bonds. The three amino groups available for site-selective acylation, Gly^{A1}, Phe^{B1}, and Lys^{B29}, are indicated. (B) Insulin–Fc conjugate. Chemical structures marked in the dashed box show alkynyl insulin analogs (**3a**–**3c**) for the conjugation. (C) The synthetic route for insulin analogs **3a**–**3c**.

This journal is © The Royal Society of Chemistry 2026

as shown in Fig. S11–S15. It is noted that other protecting groups, such as *N*-trifluoroacetyl (Tfa), have also been adapted for insulin protection by Liu *et al.*, but the final deprotection was accomplished by the strong base in an aqueous solution (15% NH_4OH or 25 mM NaOH), which renders a risk of base-catalyzed peptide hydrolysis.[32]

To validate the accuracy of the acylation site on insulin, we analyzed the insulin analogs **3a–3c** by liquid chromatography mass spectrometry (LC-MS) and peptide mapping. First, insulin and analogs **3a–3c** were reduced by the reducing agent TCEP to break the disulfide bonds, and the individual chains were analyzed by LC-MS. As shown in Fig. 2, the chromatographs of all analogs show only one right-shifted peak compared with the native chains A and B of insulin, indicating the selective acylation of only one chain. The conclusion was further confirmed by ESI-MS analysis of shifted chain peaks (Fig. S1). It is interesting to find that acylation at Phe^{B1} and Lys^{B29} shows a dramatic difference in the retention time, suggestive of a position effect on the peptide hydrophobicity. Next, insulin and **3a–3c** were digested with endoproteinase Glu-C, and the digestion mixtures were analyzed by high-resolution mass spectrometry (HRMS). As shown in Fig. 3, Glu-C can specifically cleave after glutamic acid in sequences, which truncates insulin into four peptide fragments while leaving the disulfide bonds intact.[33] For each analogue, HRMS could identify the *m*/*z* of the expected alkyne-bearing fragment, together with the other three unmodified ones (Table S1). Collectively, these results demonstrate that we have successfully acylated the insulin at the indicated site, and all the analogs contain an alkyne building block for downstream conjugation with the azido-functionalized Fc protein.

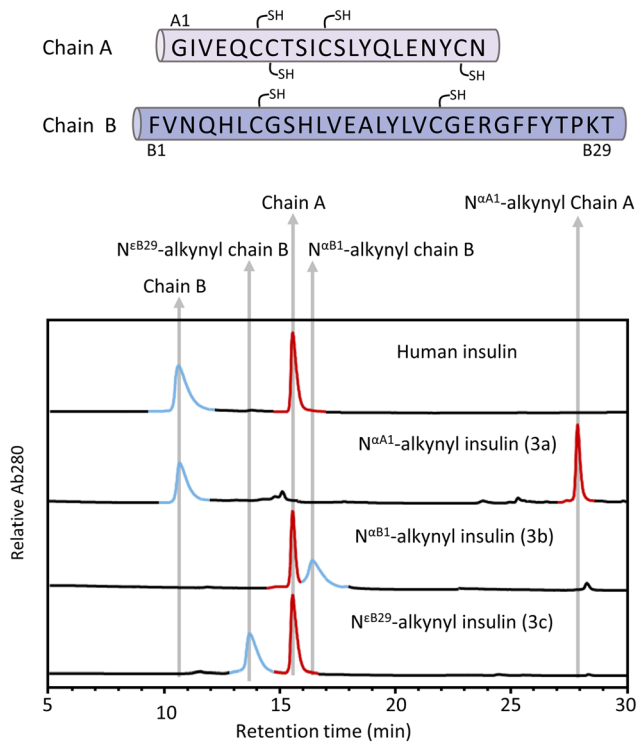

Fig. 2 HPLC analysis of reduced human insulin and its acylated analogs. Insulin and its analogs were reduced with TCEP to break the disulfide bonds in chains. Two peptide chains were then analyzed by HPLC to evaluate the acylation selectivity.

Conjugating insulin with Fc proteins

Here, we pursued a monovalent conjugate—one insulin per Fc—with an assumption of balancing the potency and duration. To obtain insulin–Fc conjugates with monovalence, we adopted a Cu^{+}-catalyzed click reaction (CuAAC) to conjugate alkyne-acylated insulin with azido functionalized Fc protein. A practical challenge, however, is that native Fc protein is expressed as a homodimer. Fc azidation by either the sortase A ligation or non-canonical amino acid incorporation strategy generally yields bivalent conjugates. To solve the problem, we implemented a single-chain Fc (scFc) strategy to construct a mono-azido Fc protein for insulin conjugation (Fig. 4A). The scFc format has previously been adapted to improve the PK performance of protein therapeutics.[34] In our design, two Fc domains were genetically connected by a 63aa loop. We have previously demonstrated the feasibility of this 63aa loop in the preparation of single-chain Fab (scFab).[35] Because Fab has a similar molecular weight and geometry to Fc, we believed that this method could be adopted for the scFc construction. This loop linker contains a large number of glycine and serine (GS) to ensure flexibility, and also covers a linear distance of ~145 Å to ensure the correct folding of Fc domains. Four clusters of three histidine residues (His × 3) are spatially inserted into the loop for scFc purification. At the loop termini, two recognition sites of tobacco etch virus (TEV) protease are incorporated to flank the linker for loop removal.

To minimize the immune response, scFc was expressed in the bacterial system to afford an aglycosylated protein, which minimizes recognition by Fc gamma receptors (FcγRs) but preserves FcRn-mediated recycling function for half-life extension.[36] After purification, the 63aa loop was cleaved by TEV to yield Fc bearing a triglycine N-terminus. Azido Fc was prepared by coincubation of the triglycyl Fc with substrate azide-LPET*GG (* represents an ester linkage to enhance ligation turnover), a step well-known as sortase A ligation. The generation of azido Fc was monitored by SDS-PAGE (Fig. 4B) after labeling azido Fc with sulfo Cy3-DBCO (Fig. S2). Azido Fc was then conjugated with alkyne insulin **3a–3c** *via* a standard CuAAC protocol.[37] By controlling the stoichiometry, azido Fc could be nearly completely consumed. Protein A affinity chromatography then removes the excess insulin and small-molecule reagents in the reaction, yielding a pure product. Anti-Fc western blotting analysis confirmed that the purified **3c**–Fc has no detectable band of azido Fc (Fig. S3), indicating the absence of Fc contamination. Size-exclusion chromatography (SEC) confirms the absence of unconjugated insulin in the purified products (Fig. 4C). Circular dichroism (CD) analysis reveals a slight increase in α-helical content after insulin conjugation relative to azido Fc, indicating the successful insulin conjugation with Fc protein (Fig. 4D, Table S2).

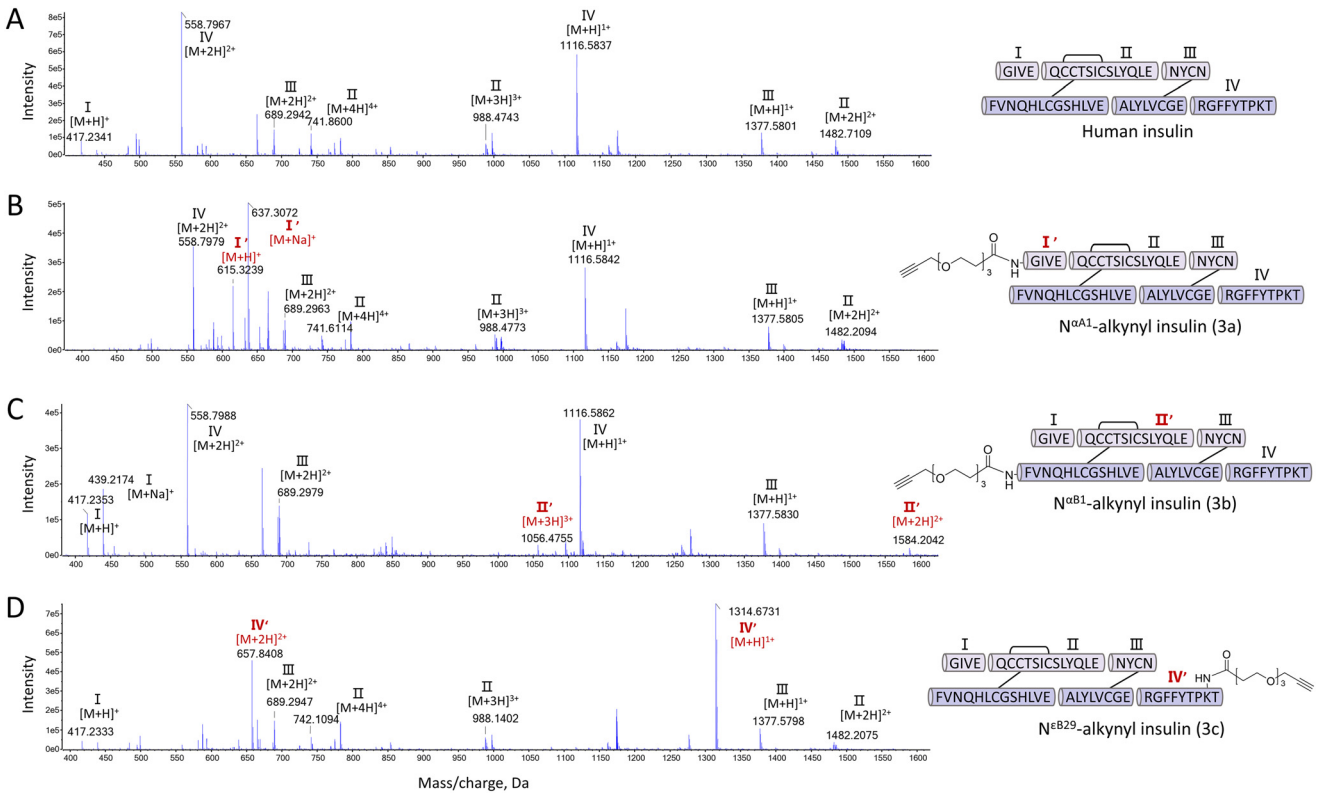

Fig. 3 Peptide mapping of insulin and its analogs after Glu-C digestion. Human insulin (A), **3a** (B), **3b** (C), and **3c** (D) were digested with endoproteinase Glu-C, and the digestion mixtures were analyzed by high-resolution mass spectrometry (HRMS). The expected alkyne-acylated fragments are highlighted in red.

Position effect on potency

To determine whether insulin analogs and insulin–Fc conjugates preserve the bioactivity of insulin, we assessed the insulin receptor (IR) pathway activation in HepG2 cells by probing Akt phosphorylation at Ser473. Akt phosphorylation is a canonical downstream event of insulin receptor signaling, and it is convenient for semi-quantification by using an anti-pAKT^{S473} antibody in the western blotting experiment.[38,39] Across three mono-alkynylated insulin analogs (**3a**–**3c**), Akt phosphorylation levels after treatment are almost consistent with the native insulin, indicating that alkyne acylation has negligible effect on insulin-stimulated Akt signaling (Fig. 5A). In contrast, Fc conjugation has a pronounced impact on Akt phosphorylation. For example, insulin–Fc conjugation at Lys^{B29} (**3c**–Fc) retains the Akt phosphorylation response, whereas the activities of **3a**–Fc and **3b**–Fc were markedly attenuated.

The observation could be explained by the structural analysis of the insulin receptor/insulin complex (PDB code: 6CEB).[40] According to the 3D complex structure, the N-termini of insulin, particularly the chain A, lie in close proximity to the receptor's α-CT segment and the L1 domain. Consequently, conjugation of a bulky Fc at A1 is expected to impose a steric hindrance that may affect the receptor engagement.[14] Impact of conjugation at B1, however, is likely spacer-dependent rather than position-forbidden: PEG-spaced insulin–Fc conjugates at B1 (PEG linker ~3.4 kDa) have been reported to retain measurable potency.[41] In this study, Lys^{B29} at the C-terminus of chain B appears to be tolerable for Fc conjugation.

To better illuminate the position effect, we evaluated the Akt phosphorylation by treating HepG2 cells with increasing concentrations of insulin and **3c**–Fc, respectively. As shown in Fig. 5B and Fig. S4, **3c**–Fc exhibits a reduced apparent potency relative to insulin in the HepG2 pAkt assay (36.4 nM *vs.* 2.8 nM). Such potency attenuation is not a disadvantage for basal insulin therapy, because the attenuated activity of insulin can slow down the receptor-mediated clearance and support a flatter PD profile.

It is worth noting that HepG2 cells express not only the insulin receptor (IR), but also the insulin-like growth factor 1 receptor (IGF1R), and IR/IGF1R hybrid receptors. Moreover, the prolonged stimulation (6 h or 24 h), albeit with results of stronger pAKT signals, may reflect differences in ligand stability, receptor trafficking, and other secondary cellular effects. The quantitative data of pAkt assay here could not be interpreted as a direct measure of insulin potency. To minimize the impact, we performed a series of short-term stimulations and analyzed Akt phosphorylation by western blotting. As shown in Fig. 5C, native insulin could induce rapid Akt phosphorylation at a concentration of 100 nM. In comparison, the treatment with 100 nM of **3c**–Fc shows a gradual response of Akt phosphorylation, indicating the involvement of secondary cellular effects. To better evaluate the activity, we chose the **3c**–Fc concentration of 1000 nM,

 This journal is © The Royal Society of Chemistry 2026

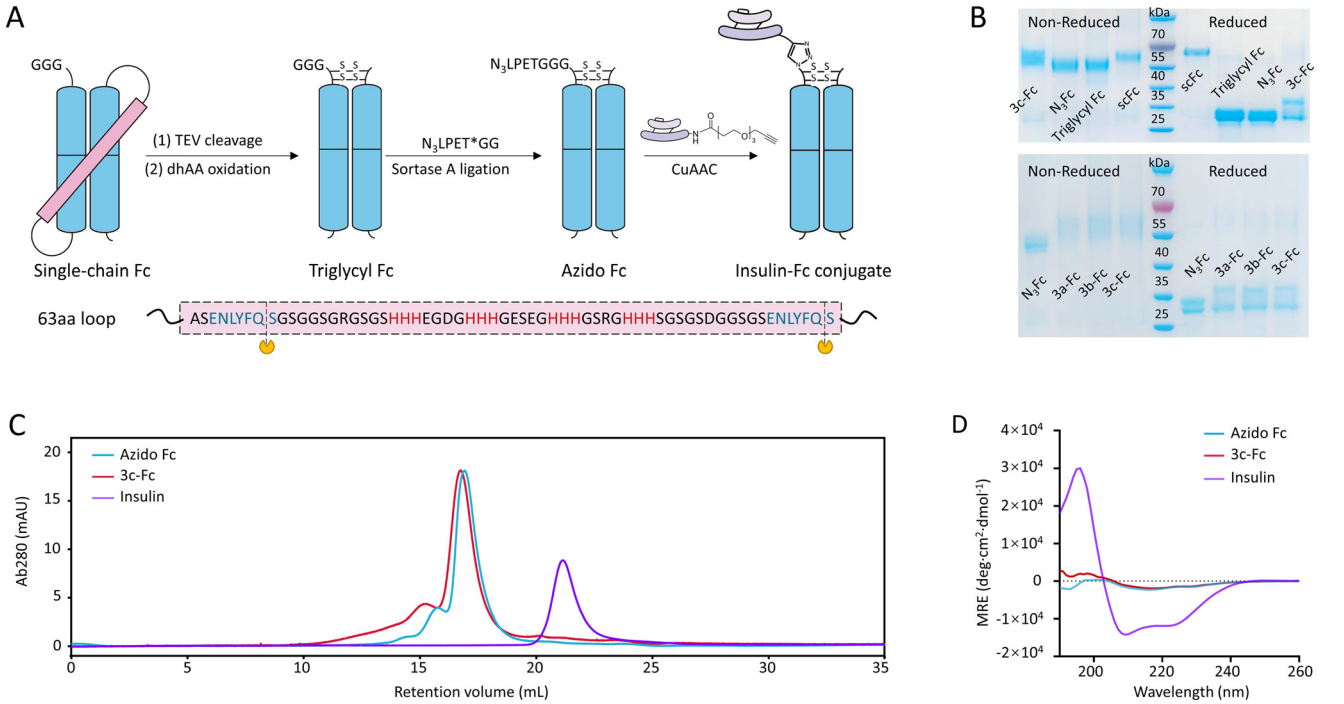

Fig. 4 Preparation and characterization of azido Fc and insulin–Fc conjugates. (A) Schematic illustration of insulin–Fc conjugates prepared from the single-chain Fc (scFc) precursor. After TEV cleavage, dhAA oxidation, and sortase A ligation, the monovalent azido Fc was obtained, and then conjugated with alkyne-acylated insulin by the CuAAC reaction. The 63aa loop contains two epitopes (blue) for TEV cleavage and four histidine clusters (red) for the Ni-NTA purification. (B) SDS–PAGE analysis of Fc variants (upper) and insulin–Fc conjugates (bottom) under non-reduced and reduced conditions. (C) SEC chromatograms of insulin, azido Fc, and **3c**–Fc obtained with the TSKgel SuperSW mAb HR column. (D) Far-UV circular dichroism spectra of insulin, azido Fc, and **3c**–Fc.

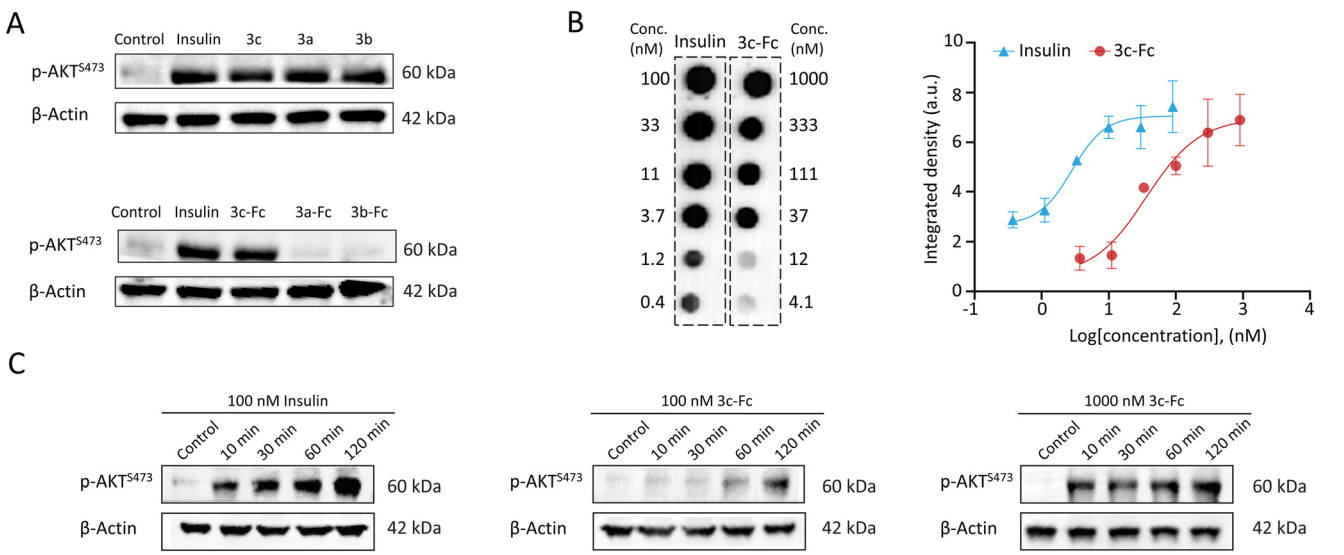

Fig. 5 *In vitro* pAkt assay of insulin analogs and insulin–Fc conjugates. (A) Western blot analysis of Akt phosphorylation at Ser473 in HepG2 cells treated with insulin, alkynylated insulin analogs (**3a**–**3c**) or insulin–Fc conjugates (**3a**–Fc, **3b**–Fc, and **3c**–Fc) at 100 nM for 6 h. (B) Dot blot analysis and concentration–response fitting of Akt phosphorylation in HepG2 cells treated with serial dilutions of insulin or **3c**–Fc for 24 h. (C) Western blot analysis of Akt phosphorylation in HepG2 cells treated with 100 nM insulin, 100 nM **3c**–Fc, or 1000 nM **3c**–Fc for 10, 30, 60, and 120 min. Uncropped immunoblot images are provided in the SI.

which previously produces responses comparable to 100 nM of insulin in the dot blotting assay. A more instant response was observed, indicating the direct activation of the insulin signaling pathway (Fig. 5C, right panel). Taken together,

these results indicate that the impact of Fc conjugation on insulin potency is site-dependent. Compared to other amino ends, Lys^{B29} is more tolerable in the function. Its conjugate **3c**–Fc was selected for the subsequent *in vivo* pharmacodynamic evaluation.

In vivo basal insulin therapy

We next proceed to the *in vivo* evaluation for basal insulin therapy. In alloxan-induced diabetic mice, native insulin and its acylated analog **3c** exhibit nearly superimposable glucose-lowering kinetics, indicating that the alkyne handle does not measurably perturb insulin pharmacodynamics *in vivo* (Fig. 6A). In contrast, its Fc conjugate, **3c**–Fc, displays a slower onset but more sustained glucose control, with glycemia remaining significantly lower than that of insulin after 2 h (Fig. 6B), indicating that Fc conjugation can flatten the insulin response toward a basal-leaning profile. The pharmacodynamic effect is consistent with the pharmacokinetics of two insulin agents. As shown in Fig. 6C, the blood concentration of insulin peaks at ~1 h and returns to baseline within ~3 h, whereas **3c**–Fc displays a flatter and more sustained exposure–time course. The result confirms that insulin–Fc has a long pharmacokinetic profile to minimize variability in plasma exposure. Insulin degludec is included in the pharmacodynamic experiment as a clinically relevant basal insulin benchmark. At the same dose, insulin degludec also produces a sustained glucose-lowering effect.

The dose escalation experiment shows a clear exposure–duration relationship. The increased dose of **3c**–Fc progressively extends the window of normoglycemia. At 200 nmol kg^{-1} (s.c.), **3c**–Fc maintains the normoglycemic status over 11.5 h, and the glucose-lowering effect could be seen even at the end of the experiment (20 h) (Fig. 6D). In healthy mice, **3c**–Fc (100 nmol kg^{-1}, s.c.) yields a significantly lower hypoglycemia index than insulin (Fig. 6E), consistent with the notion that the increase of

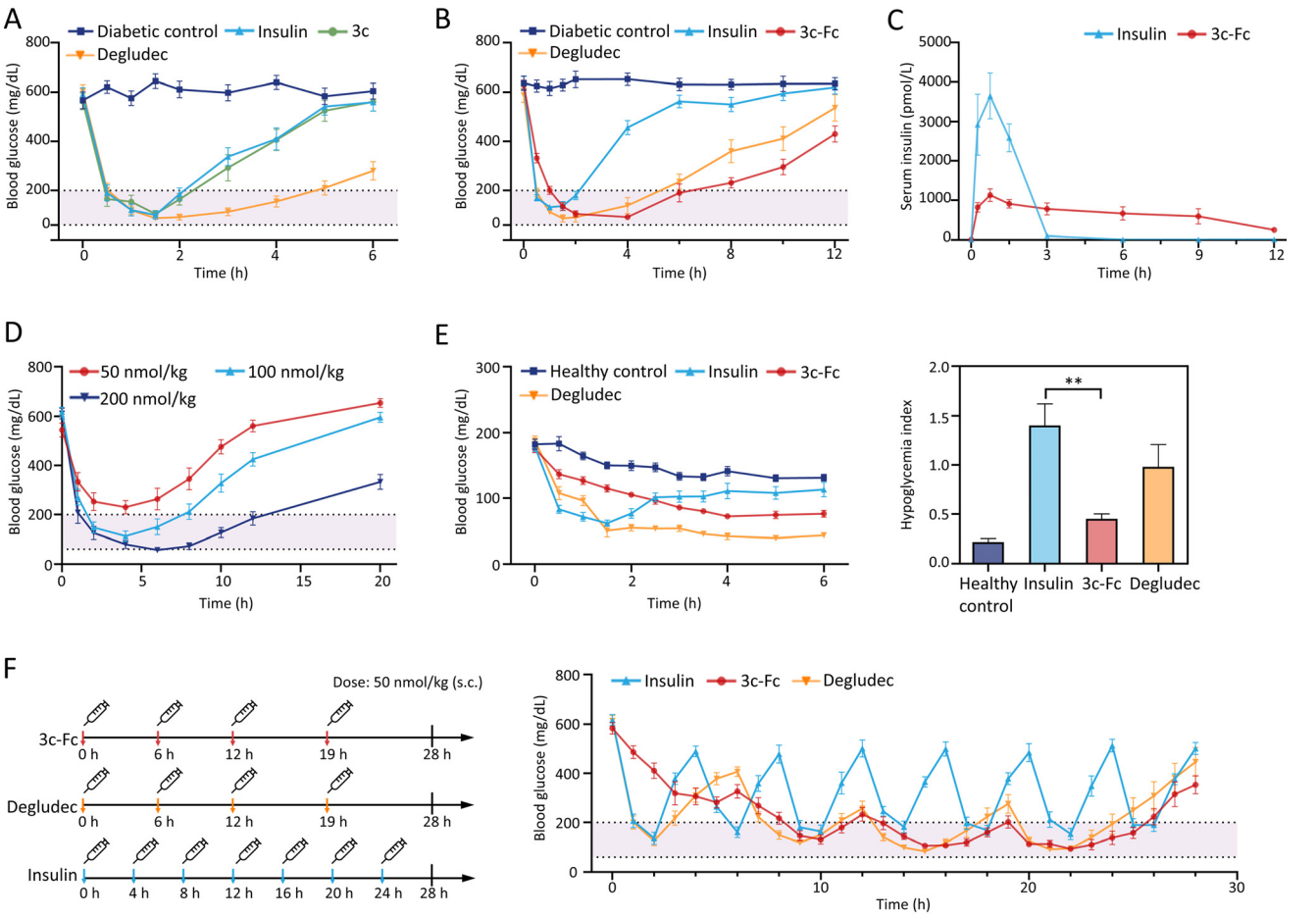

Fig. 6 *In vivo* basal insulin therapy in alloxan-induced diabetic mice. (A) Blood glucose profiles of alloxan-induced diabetic mice treated with PBS, insulin, **3c**, or insulin degludec at a single dose of 100 nmol kg^{-1} (s.c.). (B) Blood glucose profiles of alloxan-induced diabetic mice treated with PBS, insulin, **3c**–Fc, or insulin degludec at a single dose of 100 nmol kg^{-1} (s.c.). (C) Pharmacokinetic profiles of insulin and **3c**–Fc in mice by monitoring the insulin decay using the anti-human insulin ELISA kit. (D) Dose-dependent blood glucose control in diabetic mice treated with **3c**–Fc at 50, 100, or 200 nmol kg^{-1} (s.c.). (E) Blood glucose profiles of healthy mice treated with PBS, insulin, **3c**–Fc, or insulin degludec at 100 nmol kg^{-1} (s.c.) and the corresponding hypoglycemia index. (F) Long-term glucose control in diabetic mice by multiple doses of insulin, **3c**–Fc, or insulin degludec at 50 nmol kg^{-1} (s.c.) according to the indicated dosing regimens. The normoglycemic range was indicated by a purple-filled box. Data are presented as mean ± SEM (n = 7 per group). Individual animal traces are provided in Fig. S6. $^{*}P < 0.05$, $^{**}P < 0.01$.

This journal is © The Royal Society of Chemistry 2026

the molecular size can slow down the subcutaneous absorption and prolong the insulin exposure.[42] By comparison, insulin degludec, as a modified insulin analog with a molecular size close to native insulin, produces a more instant and superior glucose-lowering effect than **3c**–Fc, likely owing to its high potency. Within a low-dose repeat-dosing regimen (50 nmol kg^{-1}, s.c.), insulin requires subcutaneous injections every 4 h to maintain a suboptimal glycemic control, whereas **3c**–Fc achieves a more durable pharmacodynamic profile with only four injections over 28 h, with even a better sustenance than the profile observed by insulin degludec, demonstrating a tangible reduction in the dosing frequency (Fig. 6F).

To assess whether **3c**–Fc can maintain glycemic control after the diet, we sequentially performed the glucose tolerance test and feeding challenge.[42,43] In the first intraperitoneal glucose tolerance test (IPGTT), mice treated with both insulin and **3c**–Fc quickly return to near-normoglycemia. The pharmacodynamic response is comparable to that of the healthy control mice. However, **3c**–Fc retains the capacity to normalize glycemia in the subsequent round of IPGTT, whereas insulin progressively loses efficacy (Fig. 7A). In the feeding challenge experiment, a similar trend was observed (Fig. 7B). These pharmacodynamic differences are further supported by the corresponding AUC analysis shown in the bottom panels of Fig. 7A and B. Altogether, these results demonstrate that **3c**–Fc, as a basal-leaning insulin, provides more durable glycemic coverage than native insulin during repeated glucose and feeding challenges in alloxan-induced diabetic mice; however, given the limitations of the alloxan model, further validation is needed to assess the broader applicability of these findings.

It is worth noting that the stability of insulin in the blood is the rate-limiting factor in the *in vivo* insulin basal therapy. By probing the pharmacokinetic profile of the Fc domain *via* the anti-Fc ELISA kit, we found that azido Fc and **3c**–Fc exhibit comparable Fc exposure *in vivo*, with an apparent half-life extending beyond 96 h (Fig. S5). By comparison, the insulin exposure measured by anti-insulin ELISA in Fig. 6C persists for only ~12 h. This observation is interesting, but it might be not indicative of payload degradation in the circulation, considering the difference of detection epitopes of anti-Fc and anti-insulin ELISA kits. A deep analysis of metabolites by mass spectrometry or sequencing is required to answer the question. Altogether, our study demonstrates that insulin–Fc conjugates could be an efficacious platform for basal insulin coverage.

Conclusion

In this study, we establish a modular chemical platform for constructing monovalent, site-defined insulin–Fc conjugates. Site-selective acylation of alkyne handles at Gly^{A1}, Phe^{B1}, or Lys^{B29} generated a set of insulin analogs, which can further couple with an azido Fc scaffold derived from a single-chain Fc precursor. Among the three tested conjugation sites, Lys^{B29} was the most favorable position for this specific monovalent Fc architecture, with **3c**–Fc retaining the strongest downstream Akt

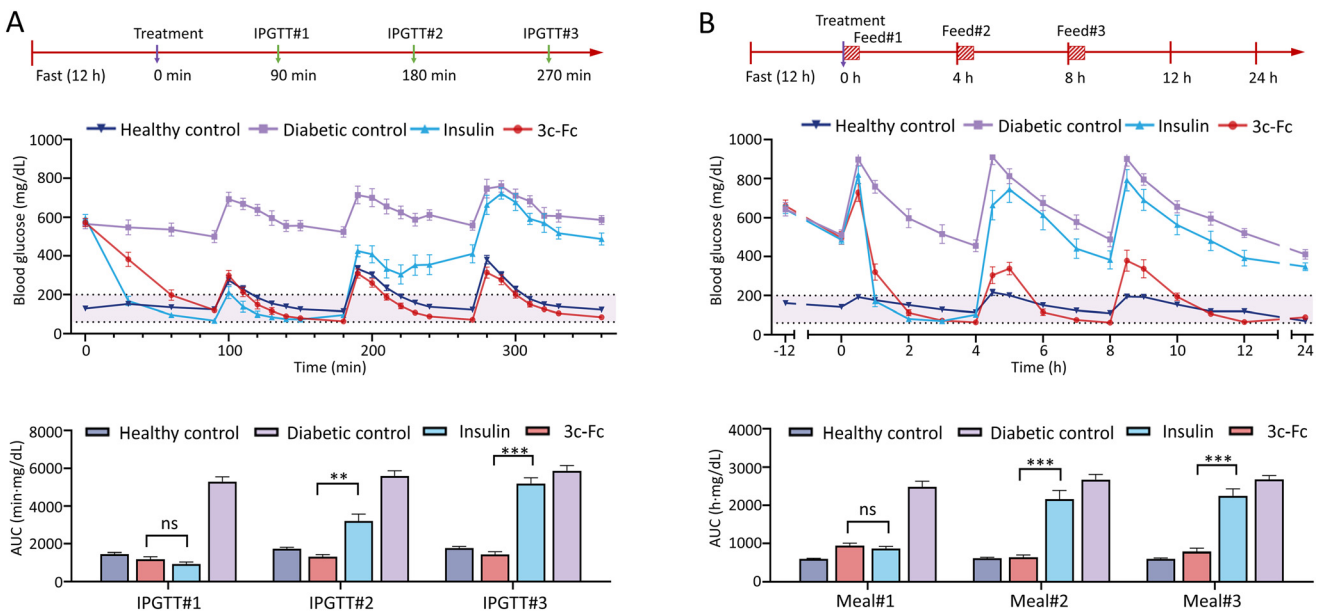

Fig. 7 Glucose and feeding challenges in alloxan-induced diabetic mice after treatment with insulins. (A) For the intraperitoneal glucose tolerance test (IPGTT), healthy control mice and diabetic control mice received PBS, whereas diabetic mice in the treatment groups received insulin or **3c**–Fc (100 nmol kg^{-1}, s.c.). Glucose (1.5 g kg^{-1}, i.p.) was administered according to the experimental timeline shown above. The lower panel shows the corresponding AUC for the three sequential IPGTT rounds. (B) For the feeding challenge, healthy control mice and diabetic control mice received PBS, whereas diabetic mice in the treatment groups received insulin or **3c**–Fc (100 nmol kg^{-1}, s.c.). At each indicated time point, mice were allowed to feed for 20 min. The lower panel shows the corresponding AUC for the three meal challenges. The purple-filled area indicates the normoglycemic range. Data are presented as mean ± SEM (n = 7 per group). Individual animal traces are provided in Fig. S7. ns, not significant; *P < 0.05; **P < 0.01; ***P < 0.001.

phosphorylation response among the Fc conjugates. *In vivo*, **3c**–Fc prolongs the glucose-lowering action of native insulin toward a more sustained, basal-leaning profile and reduces dosing frequency, with insulin degludec included as a clinically relevant basal insulin benchmark. Altogether, our results establish the insulin–Fc conjugate at Lys^{B29} as a promising long-acting insulin conjugate for further optimization. This platform also provides a generalizable route to convert short-lived peptide hormones into longer-acting therapeutics using a standardized Fc conjugation.

Materials and methods

General information

Unless otherwise noted, reagents were purchased from commercial suppliers and used as received. Human insulin was obtained from standard vendors. Human insulin was purchased from Bersee Bio (Beijing, China). Boc-NHS and alkyne-PEG_3-NHS were obtained from Aladdin Scientific (Shanghai, China). All final compounds used for biological evaluation were characterized by analytical RP-HPLC, with a purity of >95% (Fig. S8–S10). No unexpected or unusually high safety hazards were encountered in the synthetic procedures.

Site-selective acylation of insulin by alkyne-PEG_3-NHS

Mono-alkynylated insulin analogs were prepared by selective acylation of the three amino groups on insulin (Gly^{A1}, Phe^{B1}, Lys^{B29}) independently. The accessibility of these amino groups was controlled by a combined strategy of Boc protection and acylation conditions. Detailed synthetic procedures, purification conditions, and characterization data are provided in the SI.

HPLC analysis

Insulins were dissolved in 20% MeCN in water (1 mg mL^{-1}) and an aliquot (10 μL) was sampled to a reversed-phase HPLC system (Shimadzu, Japan) equipped with a WondaSil C18 Superb column (5 μm, 4.6 × 150 mm, GL sciences). Mobile phase A was H_2O containing 0.1% TFA, and mobile phase B was MeCN containing 0.1% TFA. Chromatography was performed at a flow rate of 1.0 mL min^{-1} using a gradient of 20% B for 5 min, followed by 20–95% B over 30 min, and then re-equilibration to the initial conditions (20% B). UV detection was set at 280 nm. To analyze insulin chains, insulin or its analogs were reduced by incubation with 1 mM tris(2-carboxyethyl)phosphine (TCEP) at 37 °C for 30 min. The samples were subjected to HPLC analysis. The corresponding chain peaks were confirmed by ESI–MS.

Glu-C digestion and peptide mapping

Insulin, **3a**, **3b**, and **3c** were dissolved in 50 mM ammonium bicarbonate buffer (pH 7.8) to prepare 5 mg mL^{-1} stock solutions. For digestion, 100 μg of each peptide was mixed with 10 μL of Glu-C endoproteinase (1 mg mL^{-1}, Sigma-Aldrich) and incubated at 37 °C overnight. The resulting solutions were precipitated with an equal volume of MeCN prior to analysis. High-resolution mass spectra (HRMS) were acquired on an AB Sciex TripleTOF 6600+ instrument (SCIEX, USA).

Expression and purification of single-chain Fc protein

The cDNA encoding the engineered single-chain Fc (scFc) precursor derived from human IgG1 Fc (GenBank: AF150959.1) was cloned into the pET-28a(+) expression vector using the standard molecular cloning method (scFc sequence is available in the SI). The construct was transformed into BL21(DE3) cells, and protein expression was induced using the Studier autoinduction method.[44] Bacteria were harvested by centrifugation at 8000 × *g* for 10 min and lysed using a French press homogenizer (Yonglian Biotechnology, China). After centrifugation (12 000 × *g* for 10 min), the supernatant was collected and applied to Ni-affinity chromatography. The purified scFc protein was desalted with a G-25 desalting column (Cytiva, USA) and used in the next step without further purification.

Preparation of azido Fc by sortase A ligation

The purified scFc was first treated with TEV protease at a mass ratio of 100 : 1 (scFc : TEV) at room temperature overnight to remove the 63aa linker and generate a triglycyl Fc. Without purification, the Fc protein in reaction was diluted to 5 mg mL^{-1}, and oxidized with 1 mM dehydroascorbic acid (dhAA) at 37 °C for 2 h to promote the disulfide bond reformation. The Fc protein was then buffer-exchanged into TBS (20 mM Tris-HCl, 150 mM NaCl, pH 7.4) using a G-25 column (Cytiva, USA). An azido group was ligated to the N-terminus of one Fc chain by sortase A-mediated transpeptidation using a protocol and azido substrate (azido-LPET*GG) we previously reported.[45] Briefly, triglycyl Fc (2 mg mL^{-1}) was co-incubated with azido-LPET*GG (1 mM, 25 equiv.) in the presence of 7M sortase A (200 nM) at room temperature overnight. The azido Fc fragment was isolated by Protein A affinity chromatography according to the manufacturer's protocol (Chroma, China). Elution fractions were combined, concentrated, and buffer-exchanged into PBS (137 mM NaCl, 2.7 mM KCl, 10 mM Na_2HPO_4, 1.8 mM KH_2PO_4, pH 7.4) using a G-25 column (Cytiva, USA). The purified azido Fc was stored in PBS containing 20% glycerol at −20 °C.

Insulin–Fc conjugation by CuAAC

To obtain the monovalent insulin–Fc conjugate, insulin analogs (**3a–3c**) were coupled to azido Fc by copper-catalyzed azide–alkyne cycloaddition (CuAAC). Briefly, the insulin analog (**3a**, **3b** or **3c**) was dissolved in 0.1 M Na_2CO_3 to prepare a stock solution (1 mg mL^{-1}). Azido Fc (2 mg mL^{-1} in PBS) was mixed with the corresponding insulin analog (3 equiv.), followed by addition of $CuSO_4$ (0.1 mM), THPTA (0.5 mM) and sodium ascorbate (5 mM) according to an established protocol.[37] The mixture was incubated at room temperature for 1 h and quenched with 0.5 M EDTA (10 equiv.). Products were purified by the Protein A affinity chromatography (Chroma, China), and elution fractions were buffer-exchanged into PBS using a G-25 column. The

 This journal is © The Royal Society of Chemistry 2026

purified insulin–Fc conjugates (**3a**–Fc, **3b**–Fc and **3c**–Fc) were stored in PBS containing 20% glycerol at −20 °C.

Size-exclusion chromatography

Protein samples were diluted to 3 mg mL^{-1} with the sample buffer (20 mM NaH_2PO_4, 100 mM Na_2SO_4, pH 7.4). An aliquot (20 μL) was sampled and analyzed using a Shimadzu LC-40 HPLC system with a TSKgel SuperSW mAb HR column (4 μm, 7.8 × 300 mm, TOSOH bioscience) using the same buffer as the mobile phase. The flow rate was set at 0.5 mL min^{-1}. The analysis was performed at room temperature with UV detection at 280 nm (Shimadzu, Japan).

Circular dichroism spectroscopy

The protein secondary structure was characterized by far-UV circular dichroism (CD) spectroscopy. Protein samples were dissolved in 20 mM sodium phosphate buffer (pH 7.4) at a concentration of 0.25 mg mL^{-1} and loaded into a 1 mm pathlength cuvette. Spectra were collected on a Chirascan V100 CD spectrometer over 190–260 nm (Applied Photophysics, UK). The secondary structure content was estimated using CDNN software.

Akt phosphorylation

Akt phosphorylation after insulin stimulation was performed on HepG2 cells. Briefly, HepG2 cells were cultured in RPMI 1640 (Gibco) supplemented with 10% fetal bovine serum (FBS, Gibco) and 1% penicillin–streptomycin (Gibco) at 37 °C in a humidified incubator with 5% CO_2. HepG2 cells were seeded in 6-well plates at 2.5×10^5 cells per well for 24 h, and then serum-starved overnight before stimulation. For single-dose treatment, cells were treated with insulin, alkynyl insulin analogs (**3a**–**3c**), or the corresponding Fc conjugates (**3a**–Fc, **3b**–Fc, and **3c**–Fc) at 100 nM for 6 h. For concentration titration experiments, cells were treated with serial dilutions of insulin (0.4, 1.2, 3.7, 11, 33, and 100 nM) or **3c**–Fc (4.1, 12, 37, 111, 333, and 1000 nM) for 24 h. To assess acute Akt phosphorylation and reduce the contribution of secondary effects associated with prolonged stimulation, cells were treated with 100 nM insulin, 100 nM **3c**–Fc, or 1000 nM **3c**–Fc for 10, 30, 60, and 120 min. The cell monolayer was then lysed by RIPA buffer (Beyotime) supplemented with protease and phosphatase inhibitor cocktails (Beyotime, P1081), and protein concentrations were determined by BCA assay (Thermo Scientific, A55860). The phosphorylated Akt was analyzed by western blotting.

Western blotting analysis

Equal amounts of protein (50 μg per lane) were separated by SDS–PAGE, transferred to PVDF membranes, blocked with 5% BSA in TBST for 1 h, and incubated with anti-phospho-Akt (Ser473) antibody (Abclonal, AP0140) overnight at 4 °C, followed by HRP-conjugated secondary antibody (Proteintech, SA00001–2) for 1 h at room temperature. β-Actin (Proteintech, HRP-60008) is used as the housekeeping control. Signals were developed with ECL reagent (Proteintech, PK10003) and imaged on a ChemiDoc system (Bio-Rad, USA).

For anti-Fc western blotting, purified Fc variants and **3c**–Fc were analyzed by non-reduced SDS–PAGE, transferred to PVDF membranes, and detected with an HRP-conjugated anti-human Fc antibody (Genscript, 50B4A9).

Dot blot analysis

Clarified lysates (1 μL) were adjusted to equal total protein concentration (0.1 μg μL^{-1}) based on BCA quantification, directly spotted onto PVDF membranes, and processed as described for western blotting.[46] ECL reagent was applied, and the blot image was captured using the ChemiDoc system (Bio-Rad, USA). The signal intensities were quantified by ImageJ, and apparent EC_{50} values were determined by four-parameter logistic fitting in GraphPad Prism.

In vivo pharmacodynamic studies

All animal studies were performed under the protocol approved by the Institutional Animal Care and Use Committee of Wuhan University, in accordance with the guidelines of the Chinese Regulations for the Administration of Affairs Concerning Experimental Animals. Male C57BL/6 J mice (6–8 weeks old, 20–25 g) were used for alloxan-induced type 1 diabetes model establishment by intraperitoneal injection of alloxan monohydrate (150 mg kg^{-1}) after overnight fasting. Mice with fasting blood glucose (BG) levels > 400 mg dL^{-1} were considered diabetic.

For single-dose pharmacodynamic experiments, diabetic mice (n = 7 per group) received PBS, insulin, **3c**, **3c**–Fc, or insulin degludec at 100 nmol kg^{-1} by subcutaneous injection. Blood glucose levels were monitored at the indicated time points after dosing. For dose-escalation experiments, diabetic mice received **3c**–Fc at 50, 100, or 200 nmol kg^{-1} by subcutaneous injection, and blood glucose was monitored over 20 h. For repeat-dosing experiments, diabetic mice received insulin, **3c**–Fc, or insulin degludec at 50 nmol kg^{-1} by subcutaneous injection according to the dosing schedules indicated in Fig. 6F.

For fasting hypoglycemia experiments, healthy mice (n = 7 per group) received PBS, insulin, **3c**–Fc, or insulin degludec at a dose of 100 nmol kg^{-1} under fasting conditions. The hypoglycemia index was calculated as $(BG_0 - BG_{nadir})/T_{nadir}$, where BG_0 is the initial blood glucose level before dosing, BG_{nadir} is the lowest observed blood glucose level during the monitoring period, and T_{nadir} is the time required to reach the nadir.[42]

For glucose tolerance and feeding challenge experiments, diabetic mice (n = 7 per group) received PBS, insulin, or **3c**–Fc at 100 nmol kg^{-1}, and healthy mice receiving PBS were included as a non-diabetic control group. For the glucose tolerance test, glucose was administered intraperitoneally at the dose of 1.5 g kg^{-1}. For the feeding challenge, mice were allowed to feed for 20 min at each indicated time point.

Pharmacokinetic studies

To monitor the pharmacokinetics, insulin, azido Fc and **3c**–Fc were subcutaneously injected to 12-week-old mice at a dose of 100 nmol kg^{-1}. At the indicated time points (0.1–96 h, varying between different groups), approximately 25 μL of blood was collected from the retro-orbital sinus. Blood samples were allowed to clot, and serum was isolated and stored at −80 °C until analysis. Serum levels of insulin and **3c**–Fc were quantified using a human insulin ELISA kit (Multi Science, EK9220) according to the manufacturer's instructions. Serum levels of azido Fc and **3c**–Fc were quantified using a human Fc ELISA kit (Elabscience, E-EL-H1745) according to the manufacturer's protocol.

Statistical analysis

Data are presented as mean ± SEM unless otherwise stated. Statistical analysis was performed using GraphPad Prism. AUC values and hypoglycemia index were analyzed using one-way ANOVA followed by Tukey's multiple comparisons test. $P < 0.05$ was considered statistically significant. Statistical significance was defined as ns, not significant; $^{*}P < 0.05$; $^{**}P < 0.01$; $^{***}P < 0.001$.

Author contributions

The manuscript was collaboratively written with contributions from all authors, and all authors have approved the final version of the manuscript.

Conflicts of interest

There are no conflicts to declare.

Data availability

The data supporting this article have been included as part of the supplementary information (SI).

Supplementary information: detailed synthetic procedures, purification conditions, analytical RP-HPLC and ESI-MS data, peptide mapping results, protein characterization data, raw immunoblot images, pharmacokinetic and pharmacodynamic data, and individual animal traces are available in the SI. See DOI: https://doi.org/10.1039/d6md00313c.

Acknowledgements

This work was financially supported by the National Key R&D Program of China (Grant No. 2021YFA0909900) and the National Natural Science Foundation of China (Grant No. 82273860).

References

1 I. Genitsaridi, P. Salpea, A. Salim, S. F. Sajjadi, D. Tomic, S. James, S. Thirunavukkarasu, A. Issaka, L. Chen, A. Basit, A. O. Y. Luk, R. C. W. Ma, J.-C. Mbanya, A. Ramachandran, S. H. Wild, B. B. Duncan, E. J. Boyko and D. J. Magliano, *Lancet Diabetes Endocrinol.*, 2026, **14**, 149–156.
2 American Diabetes Association Professional Practice Committee, *Diabetes Care*, 2025, **48**, S181–S206.
3 A. Philis-Tsimikas, J. Aberle, H. Bajaj, I. Lingvay, Y. Mu, S. Shaikh, A. Vianna, H. Watada and S. Del Prato, *Drugs*, 2025, **85**, 1253–1268.
4 T. B. Kjeldsen, F. Hubálek, C. U. Hjørringgaard, T. M. Tagmose, E. Nishimura, C. E. Stidsen, T. Porsgaard, C. Fledelius, H. H. F. Refsgaard, S. Gram-Nielsen, H. Naver, L. Pridal, T. Hoeg-Jensen, C. B. Jeppesen, V. Manfè, S. Ludvigsen, I. Lautrup-Larsen and P. Madsen, *J. Med. Chem.*, 2021, **64**, 8942–8950.
5 B. Silver, K. Ramaiya, S. B. Andrew, O. Fredrick, S. Bajaj, S. Kalra, B. M. Charlotte, K. Claudine and A. Makhoba, *Diabetes Ther.*, 2018, **9**, 449–492.
6 P. Kurtzhals, E. Nishimura, H. Haahr, T. Høeg-Jensen, E. Johansson, P. Madsen, J. Sturis and T. Kjeldsen, *Trends Pharmacol. Sci.*, 2021, **42**, 620–639.
7 A. N. Zaykov, J. P. Mayer and R. D. DiMarchi, *Nat. Rev. Drug Discovery*, 2016, **15**, 425–439.
8 M. P. Knadler, T.-H. Nguyen, K. Campanale, M. J. De Veer, J. M. Beals, S. Li, R. Hansen, A. Siesky, M. D. Michael and C. J. H. Porter, *Pharm. Res.*, 2016, **33**, 2920–2929.
9 W. R. Strohl, *BioDrugs*, 2015, **29**, 215–239.
10 J. T. Sockolosky and F. C. Szoka, *Adv. Drug Delivery Rev.*, 2015, **91**, 109–124.
11 W. Deng, Z. Zhao, T. Zou, T. Kuang and J. Wang, *Diabetes, Metab. Syndr. Obes.: Targets Ther.*, 2024, **17**, 343–362.
12 Y. Shen, A. Joachimiak, M. R. Rosner and W. J. Tang, *Nature*, 2006, **443**, 870–874.
13 R. E. Hulse, L. A. Ralat and T. Wei-Jen, *Vitam. Horm.*, 2009, **80**, 635–648.
14 P. De Meyts, *BioEssays*, 2015, **37**, 389–397.
15 E. Nishimura, L. Pridal, T. Glendorf, B. F. Hansen, F. Hubálek, T. Kjeldsen, N. R. Kristensen, A. Lützen, K. Lyby, P. Madsen, T. Pedersen, R. Ribel-Madsen, C. E. Stidsen and H. Haahr, *BMJ Open Diabetes Res. Care*, 2021, **9**, e002301.
16 I. Jonassen, S. Havelund, T. Hoeg-Jensen, D. B. Steensgaard, P.-O. Wahlund and U. Ribel, *Pharm. Res.*, 2012, **29**, 2104–2114.
17 Y. Yamaguchi, M. Takenaga, A. Kitagawa, Y. Ogawa, Y. Mizushima and R. Igarashi, *J. Controlled Release*, 2002, **81**, 235–249.
18 J. S. Moyers, R. J. Hansen, J. W. Day, C. D. Dickinson, C. Zhang, X. Ruan, L. Ding, R. M. Brown, H. E. Baker and J. M. Beals, *J. Pharmacol. Exp. Ther.*, 2022, **382**, 346–355.
19 C. Faust, C. Ochs, M. Korn, U. Werner, J. Jung, W. Dittrich, W. Schiebler, R. Schauder, E. Rao and T. Langer, *Protein Eng., Des. Sel.*, 2020, **33**, gzaa026.
20 Q. X. Hua, S. H. Nakagawa, W. Jia, K. Huang, N. B. Phillips, S. Q. Hu and M. A. Weiss, *J. Biol. Chem.*, 2008, **283**, 14703–14716.
21 X. Chen, J. L. Zaro and W. C. Shen, *Adv. Drug Delivery Rev.*, 2013, **65**, 1357–1369.
22 R. N. Bergman, M. Kabir and M. Ader, *Int. J. Mol. Sci.*, 2022, **23**, 1826.
23 S. M. Najjar and G. Perdomo, *Physiology*, 2019, **34**, 198–215.

 This journal is © The Royal Society of Chemistry 2026

24 M. Zhao, Z.-l. Wan, L. Whittaker, B. Xu, N. B. Phillips, P. G. Katsoyannis, F. Ismail-Beigi, J. Whittaker and M. A. Weiss, *J. Biol. Chem.*, 2009, **284**, 32178–32187.

25 T. M. Tagmose, K. M. Pedersen, L. Pridal, C. E. Stidsen, M. Pedersen, Z. Lin, Y. Zhang, Z. Wan, M. Ferreras, H. Naver, P. K. Nielsen, Z. Cao, Y. Wang, L. Lykke, J. L. Christensen, V. S. Jensen, V. Manfè, T. Pedersen, E. Johansson, P. Madsen, J. T. Kodra, M. Münzel, L. De Maria, E. Nishimura and T. B. Kjeldsen, *J. Med. Chem.*, 2022, **65**, 2633–2645.

26 M. Østergaard, N. K. Mishra and K. J. Jensen, *Chem. – Eur. J.*, 2020, **26**, 8341–8357.

27 A. Fryszkowska, C. An, O. Alvizo, G. Banerjee, K. A. Canada, Y. Cao, D. DeMong, P. N. Devine, D. Duan, D. M. Elgart, I. Farasat, D. R. Gauthier, E. N. Guidry, X. Jia, J. Kong, N. Kruse, K. W. Lexa, A. A. Makarov, B. F. Mann, E. M. Milczek, V. Mitchell, J. Nazor, C. Neri, R. K. Orr, P. Orth, E. M. Phillips, J. N. Riggins, W. A. Schafer, S. M. Silverman, C. A. Strulson, N. Subramanian, R. Voladri, H. Yang, J. Yang, X. Yi, X. Zhang and W. Zhong, *Science*, 2022, **376**, 1321–1327.

28 S. B. Boga, S. W. Krska, S. Lin, D. Pissarnitski, L. Yan, A. Kekec, W. Tang, N. A. Pierson, C. A. Strulson, E. Streckfuss, X. Zhu, X. Zhang, T. Kelly and C. A. Parish, *Bioconjugate Chem.*, 2019, **30**, 1127–1132.

29 Y. Nakatani, Z. Ye, Y. Ishizue, T. Higashi, T. Imai, I. Fujii and M. Michigami, *Mol. Pharmaceutics*, 2022, **19**, 2279–2286.

30 D. H. Kim, M. Blacker and J. F. Valliant, *J. Med. Chem.*, 2014, **57**, 3678–3686.

31 T. B. Kjeldsen, F. Hubálek, T. M. Tagmose, L. Pridal, H. H. F. Refsgaard, T. Porsgaard, S. Gram-Nielsen, L. Hovgaard, H. Valore, M. Münzel, C. U. Hjørringgaard, C. B. Jeppesen, V. Manfè, T. Hoeg-Jensen, S. Ludvigsen, P. K. Nielsen, I. Lautrup-Larsen, C. E. Stidsen, E. M. Wulff, P. W. Garibay, J. T. Kodra, E. Nishimura and P. Madsen, *J. Med. Chem.*, 2021, **64**, 616–628.

32 F. Liu, W. D. Kohn and J. P. Mayer, *J. Pept. Sci.*, 2012, **18**, 336–341.

33 A. A. A. Smith, C. L. Maikawa, G. A. Roth and E. A. Appel, *Org. Biomol. Chem.*, 2020, **18**, 4371–4375.

34 L. Zhou, H. Y. Wang, S. Tong, C. T. Okamoto, W. C. Shen and J. L. Zaro, *Biomaterials*, 2017, **117**, 24–31.

35 R. Xu, Y. Zheng and W. Tai, *Biomaterials*, 2025, **313**, 122798.

36 L. C. Simmons, D. Reilly, L. Klimowski, T. S. Raju, G. Meng, P. Sims, K. Hong, R. L. Shields, L. A. Damico, P. Rancatore and D. G. Yansura, *J. Immunol. Methods*, 2002, **263**, 133–147.

37 V. Hong, S. I. Presolski, C. Ma and M. G. Finn, *Angew. Chem., Int. Ed.*, 2009, **48**, 9879–9883.

38 A. Tsuchiya, T. Kanno and T. Nishizaki, *Cell. Physiol. Biochem.*, 2013, **32**, 1451–1459.

39 S. Sen, R. Ali, A. Onkar, S. Verma, Q. T. Ahmad, P. Bhadauriya, P. Sinha, N. N. Nair, S. Ganesh and S. Verma, *Commun. Chem.*, 2024, **7**, 161.

40 G. Scapin, V. P. Dandey, Z. Zhang, W. Prosise, A. Hruza, T. Kelly, T. Mayhood, C. Strickland, C. S. Potter and B. Carragher, *Nature*, 2018, **556**, 122–125.

41 N. Wronkowitz, T. Hartmann, S. W. Görgens, D. Dietze-Schroeder, I. Indrakusuma, I. Y. Choi, S. H. Park, Y. M. Lee, S. C. Kwon, Y. Kang, M. Hompesch and J. Eckel, *Diabetes, Obes. Metab.*, 2017, **19**, 1722–1731.

42 D. H. Chou, M. J. Webber, B. C. Tang, A. B. Lin, L. S. Thapa, D. Deng, J. V. Truong, A. B. Cortinas, R. Langer and D. G. Anderson, *Proc. Natl. Acad. Sci. U. S. A.*, 2015, **112**, 2401–2406.

43 B. Z. Chen, L. Q. Zhang, Y. Y. Xia, X. P. Zhang and X. D. Guo, *Sci. Adv.*, 2020, **6**, eaba7260.

44 F. W. Studier, *Protein Expression Purif.*, 2005, **41**, 207–234.

45 H. Wang, J. Song, Y. Quan, J. Liu and W. Tai, *Bioconjugate Chem.*, 2024, **35**, 1459–1467.

46 C. Li, B. Jaentschke, Y. Song, J. Wang, T. D. Cyr, G. Van Domselaar, R. He and X. Li, *Nat. Protoc.*, 2010, **5**, 14–19.

This journal is © The Royal Society of Chemistry 2026